

ESTIMATION OF THE MECHANICAL PROPERTIES OF FOAMS USING DISPERSION MEASUREMENTS

N.B. Roozen, B. Verstraeten, J. Sermeus and C. Glorieux

*Katholieke Universiteit Leuven, Laboratory for Acoustics and Thermal Physics (ATF),
Department of Physics and Astronomy, Celestijnenlaan 200D 3001 Leuven, Belgium*

e-mail: bert.roozen@kuleuven.be

In porous materials the frame elasticity and its coupling with the surrounding fluid (e.g. air) are crucial for their sound absorption and transmission. In this contribution the elastic moduli of a porous material are determined. The longitudinal and shear wave velocities of a porous layer are estimated by means of a Lamb model, fitting the experimentally obtained Lamb wave velocity dispersion curves of two propagation modes, S0 and A0, measured over a frequency range up to 1400 Hz. The obtained value for the shear wave velocity is shown to be accurate and robust, whilst the extraction of the longitudinal wave velocity is hampered by a large uncertainty. Consequently, the approach allows for an accurate determination of the shear modulus, while the individual estimation of the Young's modulus and Poisson's ratio is quite challenging.

1. Introduction

In porous materials knowledge of the frame elasticity and its coupling with the fluid (e.g. air) is important for a correct description of the sound absorption and transmission of those materials. The determination of the material properties of this frame elasticity, such as the shear modulus and the Young's modulus, can be estimated on the basis of the frequency- and position dependent response due to mechanical excitation. The material parameters of the poro-visco-elastic material can be obtained by fitting a model on to the measured dispersion relationships.

This paper focusses on the fitting of a Lamb model on the measurement data, considering multiple modes simultaneously. Attention is paid to the uncertainty of the obtained material parameters.

2. Measurement test set-up

Guided wave velocity measurements were conducted in a semi-anechoic room in order to reduce noise and vibrations from the environment that might deteriorate the measurement. The poro-visco-elastic foam under investigation was a large piece of Eurocell foam, with a thickness of 5 cm. The sample was horizontally positioned as shown in Figure 1.

The mechanical excitation of the sample was realized by means of an electro dynamic shaker (Bruel&Kjaer mini-shaker type 4810), which was driven by the analog output of a data acquisition card (Roland Octa Capture UA 1010) and amplified by an audio power amplifier (Crest Audio FA601). The mini-shaker was positioned below the horizontally positioned poro-visco-elastic material sample that is tested, partly supporting the weight of the sample, as shown in Figure 1. The excitation signal was an exponential swept sine signal¹, ranging from 100 Hz to 3000 Hz in 2 seconds.

The response of the poro-visco-elastic material was measured by means of a laser Doppler vibrometer (Polytec controller OFV-5000 and Polytec laser head OFV-505), which recorded the normal velocity component of the porous material on the upper side of the horizontally positioned poro-visco-elastic material sample, along a measurement line which was chosen right above the point of excitation. In order to obtain sufficient light collection, a line of retro-reflecting tape was glued on the poro-visco-elastic material, as shown in Figure 2. The retro-reflecting tape is acoustically thin and relatively light, thus not affecting the measurements.

The detection point of the laser was varied by means of an optical arrangement that was positioned by means of a long-stroke-robot (Isotec rack, Vexta stepping motor), as shown in Figure 3. This optical arrangement was moved in horizontal direction such that the laser beam moved along the line of retro-reflecting tape that was glued on the poro-visco-elastic material. The optical arrangement also comprises a lens that focuses the laser beam on the line of retro-reflecting tape for optimal optical signal retrieval.

The signal from the laser Doppler vibrometer and the shaker excitation signal were recorded by means of a digital oscilloscope (LeCroy type 9310M, dual 300 MHz oscilloscope, 100 Ms/s, 50Kpts/ch). The dynamic range of the LeCroy type 9310M is 8 bits. The LeCroy oscilloscope was set at a sampling frequency of 25 kHz (which is relatively high as the highest frequency of excitation is 3kHz). The length of the time records was set to 2 s (50k samples), yielding a frequency resolution of 0.5 Hz.



Figure 1 Test set-up, bottom view showing the shaker excitation.

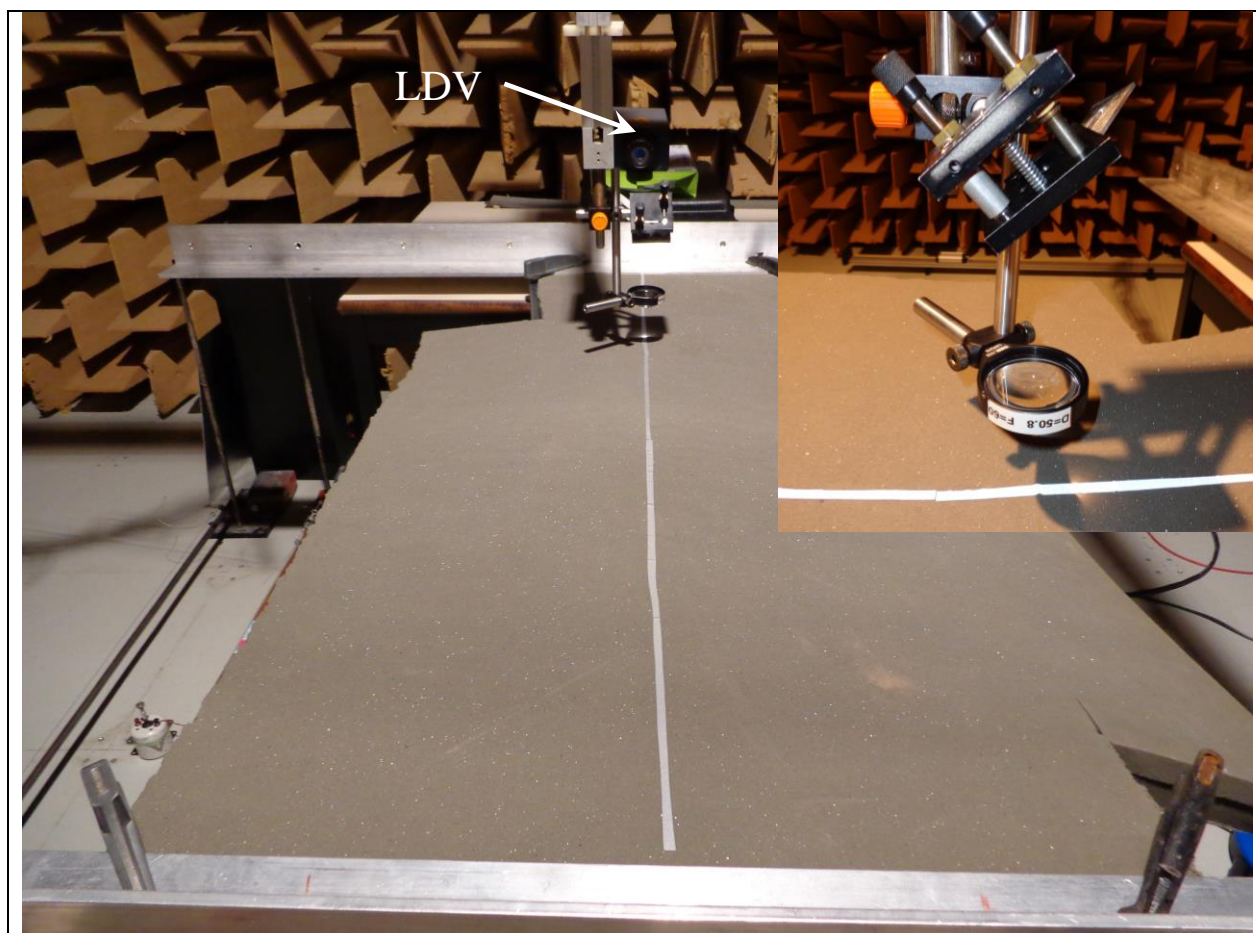


Figure 2 Test set-up, top view showing the laser Doppler vibrometer (LDV) and the optical arrangement.

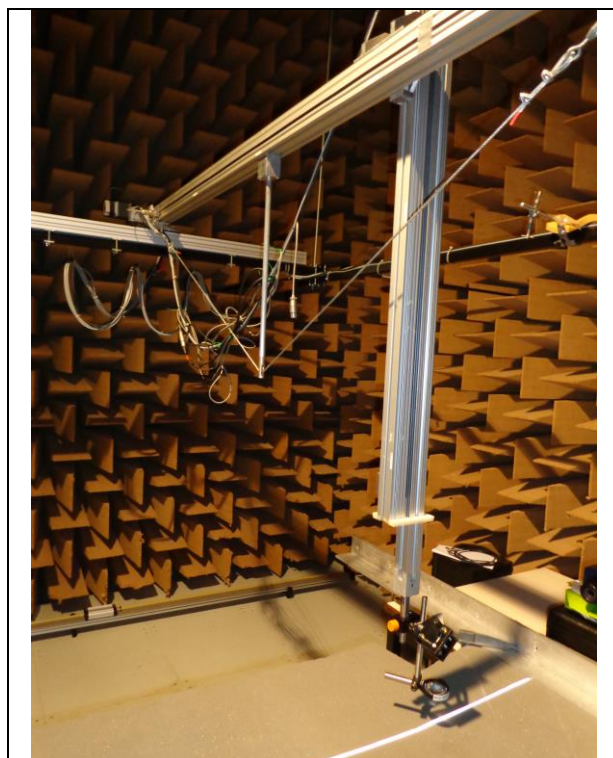


Figure 3 Optical arrangement with long-stroke robot.

The long-stroke-robot, the electro dynamic shaker and the LeCroy oscilloscope were controlled by means of a computer, running Labview 8.5. The measurement system was fully automated to allow an unattended measurement.

The total scan length was 1 m, taking measurements at each 2.5 mm, resulting in 401 measurement points. The shaker was positioned half way the scan length.

Both the velocity response time-signal of the poro-visco-elastic material and the excitation time-signal were simultaneously recorded by the digital LeCroy oscilloscope, thus enabling the determination of the response of the poro-visco-elastic material as function of frequency, using cross-spectra. No time windowing was used, as the signal was not stationary (swept sine).

3. Measurement results

The mechanical response of the porous material as function of frequency and as function of measurement position (x - ω data), $\tilde{v}(x, \omega)$, is shown in Figure 4a, where

$$\tilde{v}(x, \omega) = \int_{-\infty}^{\infty} v(x, t) e^{-i\omega t} dt, \quad (1)$$

and where $v(x, t)$ is the recorded velocity as a function of time t at position x , and where ω is the angular frequency, $\omega = 2\pi f$. Note that in practice $\tilde{v}(x, \omega)$ is obtained by means of a cross-spectral analysis of both the laser Doppler vibrometry signal and the excitation signal, thus obtaining a much better signal-to-noise ratio as a result of the averaging-process, and including both amplitude and phase information.

The response as function of the wavenumber and frequency can be obtained by taking the spatial Fourier transform of the x - ω data, to arrive at the k - ω domain:

$$\hat{\tilde{v}}(k, \omega) = \int_x \tilde{v}(x, \omega) e^{-2\pi i k x} dx, \quad (2)$$

where k is the wavenumber along the x -axis. Figure 4b shows the magnitude of the velocity in the k - ω domain.

In order to take the spatial Fourier transform in an optimum manner, without too much leakage (e.g. caused by non-periodic behaviour of the digitized signal due to the finite measurement length in the spatial domain), a Tukey window² in x -direction was applied before taking the FFT.

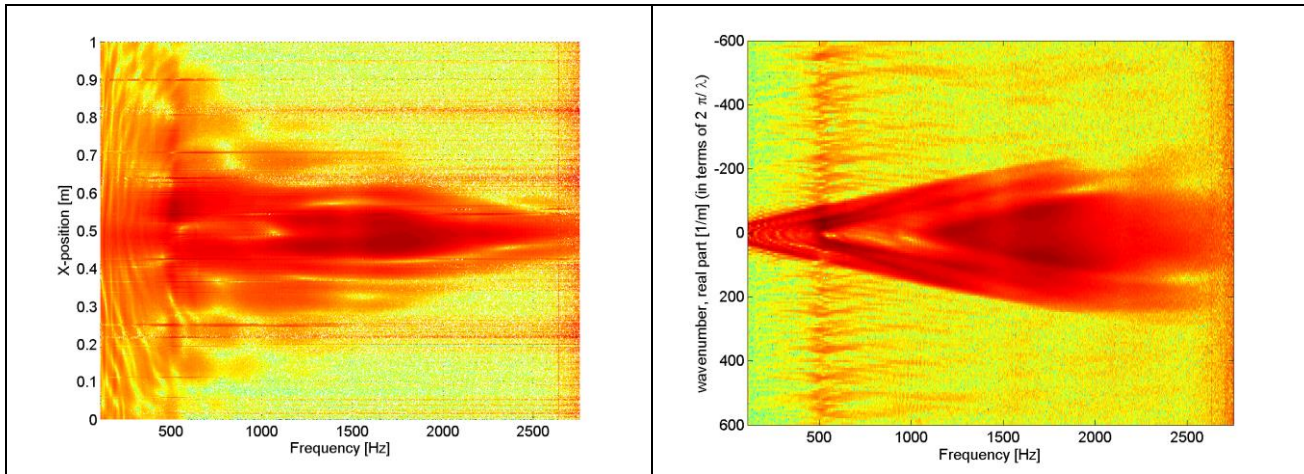


Figure 4 Dispersion measurement results as function of position and frequency (left) and as function of wavenumber and frequency (right)

Three modes were extracted from the measurement data in the k - ω domain (Figure 4b) by searching for the maximum peaks (using the Matlab routine “impoly” to define a search area around the mode of interest, searching for the maximum in this area at each frequency). Curves of maximum peak values are shown in Figure 5a. The modes are denoted by A0, S0 and A1, being the asymmetric (A) and symmetric (S) modes of the zeroth order (0) and of first order (1). The S0, A0 type and the A1-type of modes are shown in Figure 6. The lines of maximum $\hat{v}(k, \omega)$, relating the wavenumber k to the radial frequency ω are converted into propagation speeds $c(\omega)$ as function as frequency using the relationship

$$c = k/\omega \quad (3)$$

Results are shown in Figure 5b. The data points in this figure all lie on virtual lines that cross the origin $(c, \omega) = (0, 0)$, which is caused by the transformation from x - ω space to k - ω space, yielding finite resolution in k -space, $\Delta k = 1/L$, with L being the total scan length (1 m, thus $\Delta k = 1 \text{ m}^{-1}$).

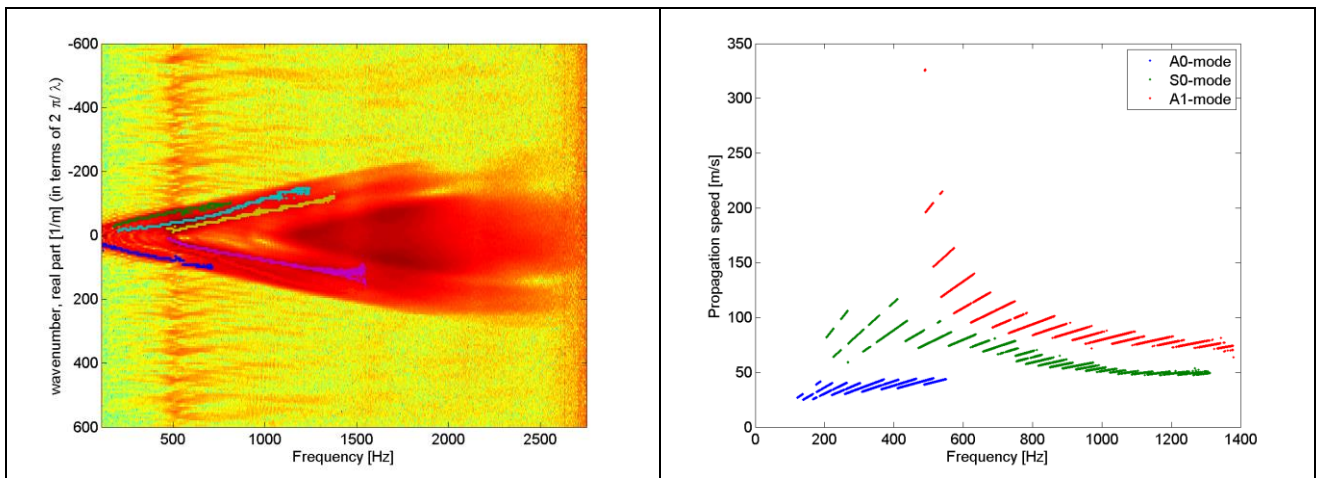


Figure 5 Dispersion measurement results as function of wavenumber and frequency, including the extraction of discrete values for the wavenumbers (left) and the extracted discrete values expressed as propagation speeds as function of frequency (employing Eq. (3)) (right)

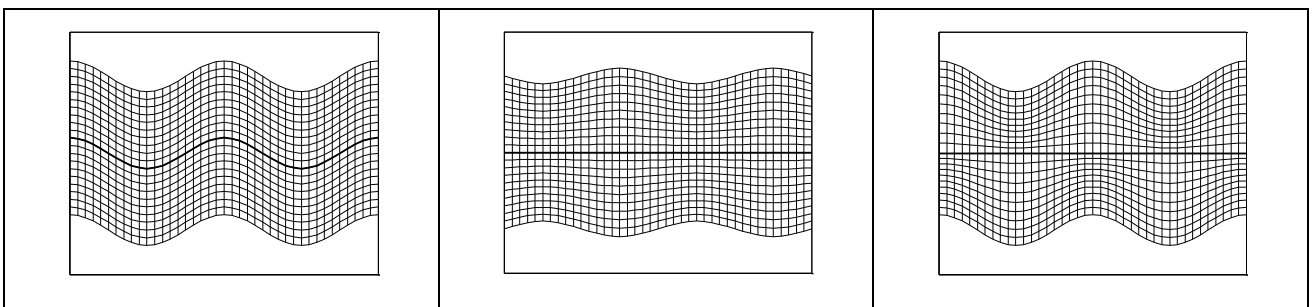


Figure 6 Snapshot of displacement field of A0-type (left), S0-type (middle) and A1-type (right) type of modes

4. Fitting by an equivalent elastic solid model

An elastic solid Lamb model as described by Viktorov^{3,4} was used to describe the propagation velocities of the longitudinal and shear wave velocities in the porous material.

The propagation velocities used in the Lamb model for longitudinal and transverse waves, c_L and c_T , respectively, were taken to be complex. We have assumed that η , the ratio of the imaginary to the real part of the propagation velocities, is equal between c_L and c_T , i.e. $\eta = \Im(c_L)/\Re(c_L)$

$=\Im(c_T)/\Re(c_T)$, where \Re denotes the real part and \Im denotes the imaginary part. The validity of this assumption is shown further on in this paper. Employing the Lamb-model, we have computed the dispersion relationships, searching for minima of the determinant that follows from the Lamb-model and the imposed boundary conditions. In order to restrict the computation time, and in view of only the real part of the wave propagation velocities being available, the roots of the determinant were sought in the (real k) - ω plane only. A search in the (complex k) - ω plane would be more accurate, but we have verified that in conditions of moderate damping, the deviation between the found roots and their exact value is quite small.

Computing the effect of variation of the model parameters $\Re(c_L)$, $\Re(c_T)$ and $\eta=\Im(c_L)/\Re(c_L)=\Im(c_T)/\Re(c_T)$, shows that $\Re(c_T)$ has the largest influence on the dispersion curve (see Figure 7). The value of $\Re(c_L)$ has much less influence. The effect of the imaginary to real part ratio parameter η is very limited (note that in Figure 7 the three parameters are varied with different variations, as mentioned in the legend). For that reason it was decided for the further fitting analysis to vary only the model parameters $\Re(c_L)$, $\Re(c_T)$ and to keep η to a fixed, arbitrary value of 0.01.

Computing the dispersion relations by means of the Lamb model, for a large range of longitudinal and shear wave velocities c_L and c_T , respectively, the cost function, expressing the fitting error can be calculated as:

$$\sum_{\omega_i} \left(\frac{c_{fit}(\omega_i) - c_{measured}(\omega_i)}{c_{measured}(\omega_i)} \right)^2 \quad (6)$$

where $c_{fit}(\omega_i)$ is the fitted phase velocity, for either the S0 or A0 mode, at angular frequency ω_i , and where $c_{measured}(\omega_i)$ is the measured propagation speed at frequency ω_i .

Minimizing this relative error for both the S0 or A0 modes simultaneously by means of an optimization, assuming the ratio of imaginary to real part of the propagation speed, η , to be equal to 0.01, gave an optimum at $\Re(c_L)=120.3$ m/s and $\Re(c_T)=49.7$ m/s. The dispersion relationship as computed by the Lamb model for the A0 and S0 modes, together with the experimentally obtained data is shown in Figure 8b (right). The cost function was calculated considering the S0 and A0-modes simultaneously.

The natural logarithm of the total error, including both the S0 and the A0 modes, is plotted in Figure 8a (left). It nicely shows the global minimum (see red circle). From Figure 8a (left) it can be seen that whilst the shear wave velocity can be determined with certain accuracy, the estimation of the longitudinal wave velocity is hampered by a large uncertainty. This uncertainty can be assessed by plotting the error as function of either c_L and c_T . As the valley of minimum error-values is nicely oriented along the c_T and c_L -axes, such a plot will give the maximum error directly (as opposed to the situation that the valley is oriented along an angle with the c_L and c_T axis, indicating a dependency of the two variables, which is not the case here). Such a plot, where the error is normalized to the minimum value of the error (i.e. the optimum) is plotted in Figure 9a and Figure 9b for the error as function of c_L and as function of c_T , respectively. The uncertainty can be determined by considering the values for c_L and c_T , respectively, where the error is a factor 2 larger than the minimum error⁵.

Using this uncertainty rule (see the circles in Figure 9 indicating the values at which the error is twice the minimum error) the estimate of the shear velocity, c_T , is 50 ± 3 m/s. The estimate of the longitudinal velocity, c_L , only has a lower limit and is given by $120 + \infty - 40$ m/s.

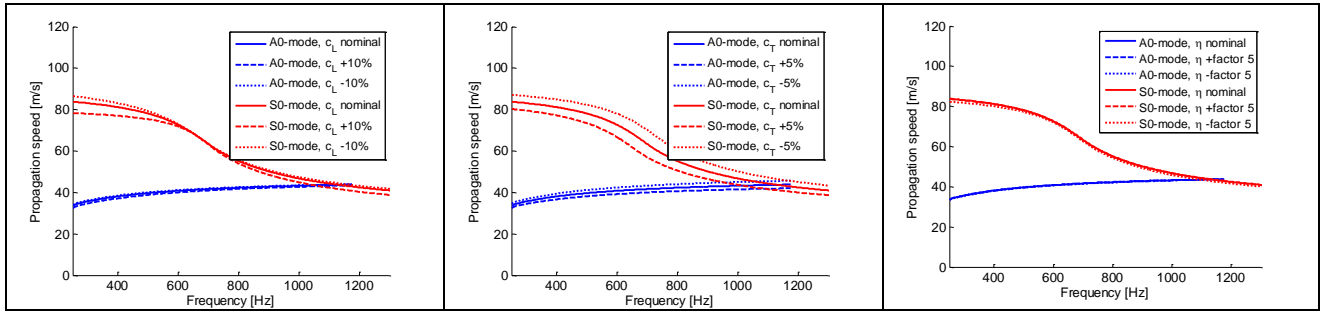


Figure 7 Effect of varying model parameters c_L (left, variation 10%), c_T (middle, variation 5%) and η (right, variation factor 5) on the dispersion relationships of A0,S0 and A1 type of modes, according to the Lamb model. Nominal values: $c_L=105.7$ m/s, $c_T=47$ m/s, $\eta=0.01$

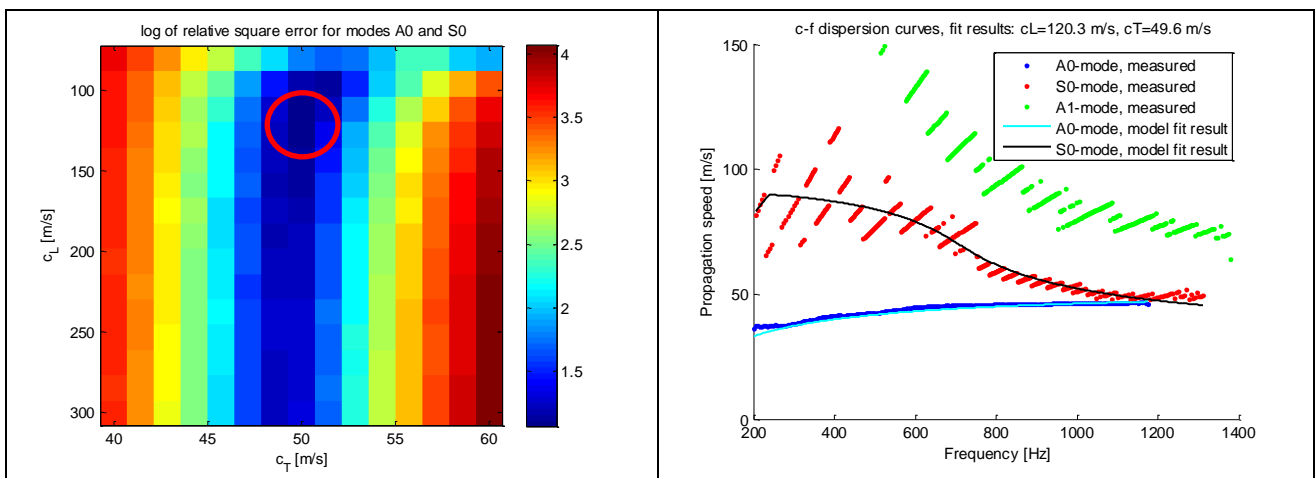


Figure 8 Error landscape as function of c_L and c_T (left) and optimization fit results: $\mathcal{R}(c_L)=120.3$; $\mathcal{R}(c_T)=49.7$; η (fixed)=0.01 (right)

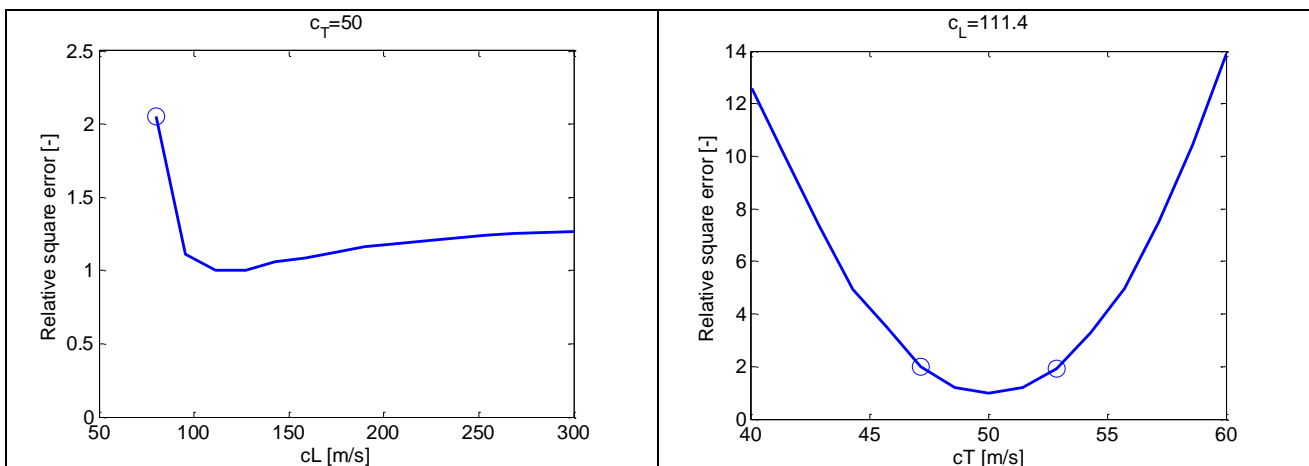


Figure 9 Normalized value of the cost function versus c_L (left) and c_T (right).

From the estimated velocity for shear waves, c_T , the shear modulus μ can be estimated as follows:

$$\mu = \rho c_T^2, \quad (7)$$

which gives $\mu = (3.11 \pm 0.37)10^5 \text{ N/m}^2$, where a density of $126 \text{ [kg/m}^3\text{]}$ was used. This density was measured by weighting the sample and measuring its volume.

The Young's modulus can also be determined from c_L and c_T :

$$\lambda = \rho (c_L^2 - 2c_T^2), \quad (8)$$

giving together with μ :

$$E = \frac{\mu (3\lambda + 2\mu)}{\lambda + \mu}. \quad (9)$$

This yields a 'fitted' value for the Young's modulus E of $8.7 \times 10^5 \text{ N/m}^2$, with a lower bound of $6.6 \times 10^5 \text{ N/m}^2$ (the value of E for $c_L=80 \text{ m/s}$ (it's lowerbound), and $c_T=49.7 - 2.9 = 46.8 \text{ m/s}$), and an undefined upper bound.

5. Conclusions

The feasibility to determine the elastic parameters of a poro-visco-elastic layer of Eurocell foam with a thickness of 5 cm from Lamb wave velocity dispersion curve was verified. The propagation velocity of shear waves, c_T , was determined to be $(50 \pm 3) \text{ m/s}$, giving a shear modulus $\mu = (3.1 \pm 0.4)10^5 \text{ N/m}^2$.

ACKNOWLEDGEMENTS

N.B. Roozen acknowledges support of the European Commission, Marie Curie Grant, FP7-PEOPLE-2011-IEF, Grant Agreement Number PIEF-GA-2011-298278, Project acronym PAM, Project title "the Physics of Acoustic Materials".

REFERENCES

- ¹ A. Farina, Simultaneous measurement of impulse response and distortion with a swept-sine technique, AES Paris convention 2000.
- ² N.B. Roozen, B. Verstraeten, L. Labelle, C. Glorieux and P. Leclaire, Advanced dispersion measurement techniques for the characterization of the mechanical properties of poro-visco-elastic materials, proceedings of Internoise 2013, Innsbruck, Austria.
- ³ I.A. Viktorov. Rayleigh and Lamb Waves; physical theory and applications. Plenum press, New York, 1967.
- ⁴ N.B. Roozen, H. Muellner, M. Rychtáriková, C. Glorieux, Influence of planking fastening on the acoustic performance of light-weight building elements: study by sound transmission and laser scanning vibrometry, submitted to Acta Acustica united with Acustica, 2014.
- ⁵ R. Salenbien, R. Côte, J. Goossens, P. Limaye, R. Labie, and C. Glorieux, Laser-based surface acoustic wave dispersion spectroscopy for extraction of thicknesses, depth, and elastic parameters of a subsurface layer: Feasibility study on intermetallic layer structure in integrated circuit solder joint, Journal of Applied Physics 109, 093104 (2011)